PHYSICAL REVIEW C **74**, 015502 (2006)

General study of superscaling in quasielastic (e, e') and (ν, μ) reactions using the relativistic impulse approximation

J. A. Caballero
Departamento de Física Atómica, Molecular y Nuclear,
Universidad de Sevilla, E-41080 Sevilla, Spain
(Received 28 March 2006; published 21 July 2006)

The phenomenon of superscaling for quasielastic lepton induced reactions at energies of a few GeV is investigated within the framework of the relativistic impulse approximation. A global analysis of quasielastic inclusive electron and charged-current neutrino scattering reactions on nuclei is presented. Scaling and superscaling properties are shown to emerge from both types of processes. The crucial role played by final state interactions is evaluated by using different approaches. The asymmetric shape presented by the experimental scaling function, with a long tail in the region of positive values of the scaling variable, is reproduced when the interaction in the final state between the knockout nucleon and the residual nucleus is described within the relativistic mean field approach. The impact of gauge ambiguities and off-shell effects in the scaling function is also analyzed.

DOI: 10.1103/PhysRevC.74.015502 PACS number(s): 25.30.Pt, 23.40.Bw, 24.10.Jv, 25.30.Fj

I. INTRODUCTION

Scaling is a very general phenomenon [1] occurring in various areas of physics that deal with probes weakly interacting with many-body systems in which a single constituent in the target system absorbs the energy and momentum transfer. The validity of the concepts of scaling [2] and superscaling [3] applied to inclusive quasielastic (QE) electron scattering at intermediate to high energies has been investigated in depth [3–5]. From an exhaustive analysis of the (e, e') world data, one concludes that the scaling behavior is highly fulfilled [4]. One may distinguish between scaling of the first kind, which corresponds to reduced cross sections being independent of the momentum transfer q, and scaling of the second kind, namely, no dependence on the nuclear species. The data analysis shows that scaling of the first kind is reasonably well respected at excitation energies below the QE peak, usually called the scaling region, whereas scaling of the second kind is excellent in the same region. The simultaneous occurrence of both kinds of scaling is named superscaling. At energies above the QE peak, where nucleon resonances are important, both types of scaling, first and, to a lesser extent, second, are broken. Scaling violations are shown to reside mostly in the transverse response, but not in the longitudinal which appears to superscale [5]. These results are in accordance with the important contributions expected in the transverse channel due to effects beyond the impulse approximation: inelastic scattering [6,7], correlations, and meson exchange currents (MEC) in both the 1p-1h and 2p-2h sectors [8–12].

The scaling analysis of QE (e, e') data was extended into the Δ region [13], leading to the extraction of two different scaling functions which embody the nuclear dynamics in the two regions. The scaling approach has been exploited to predict inclusive charged-current (CC) neutrino-nucleus cross sections. This strategy is based on the assumption that a universal scaling function exists, which is valid for both electron and neutrino scattering reactions, provided that the corresponding kinematics are similar. This hypothesis of a universal scaling function, which is true by construction in the relativistic Fermi gas (RFG) model [14], was further investigated when final state interactions (FSI) were included. The analysis performed in [15] within the context of a nonrelativistic mean field calculation, but incorporating important aspects of relativity at the level of the current operators, called the semirelativistic (SR) approach, proved that scaling properties were highly fulfilled for the electromagnetic responses at intermediate to high energies. Moreover, the scaling function extracted from these coincides with that from the (ν, μ) reaction. However, it presents a symmetric shape which is not supported by the analysis of (e, e') data. This is not unexpected because additional dynamical effects, which are beyond the nonrelativistic mean field picture considered in [15], are needed in order to reproduce the *asymmetry* extracted from the experiment.

An investigation of the QE scaling properties of CC neutrino-nucleus scattering within the context of the relativistic impulse approximation (RIA) has been presented in [16]. Although resorting only to one-body excitations, the RIA has been shown to provide the required asymmetry of the scaling function when strong relativistic potentials are included in the model. This makes an important difference with previous nonrelativistic, or SR, calculations based on the impulse approximation [15,17,18]. The superscaling function evaluated from QE (ν, μ) calculations was compared with the (e, e') phenomenological one, showing the capability of RIA models to yield the required properties of data.

In this paper we extend the investigation on scaling by performing a global analysis of (e, e') and (ν, μ) reactions within the RIA framework. We follow the general procedure of scaling and superscaling studies [5,13,15,16]. First, we calculate inclusive cross sections within a specific model and then obtain scaling functions by dividing them by the relevant single-nucleon cross sections weighted by the corresponding proton and neutron numbers [5,19]. The scaling function so

obtained is plotted against the scaling variable $\psi(q,\omega)$, and its scaling properties analyzed, i.e., we explore its dependence on the transfer momentum (first-kind scaling) and on the specific target nucleus (second-kind scaling).

A detailed study of the off-shell effects and gauge ambiguities in the scaling function is also presented. The analysis performed and its comparison with data give us important clues as to the validity of the different theoretical descriptions considered. Furthermore, the consistency between (e,e') and (ν,μ) calculations, which reflects the universality property of the superscaling function, is also clearly illustrated. Finally, we show that the RIA approach, in spite of its simplicity, gives rise to the required shape presented by the *experimental* scaling function. Scaling and superscaling ideas have been carried a step further to include neutral-current (NC) neutrino-nucleus scattering processes in [20]. Here, NC differential cross sections were obtained by making use of the *phenomenological* (e,e') scaling function, i.e., the universality property was assumed. It will be very interesting to investigate scaling for NC reactions within the RIA framework. This will allow us to prove if various RIA-FSI models superscale, and moreover, if the *universal asymmetric* scaling function also emerges from the RIA calculations on NC processes.

The paper is organized as follows. In Sec. II, we present a brief summary of the basic formalism involved in describing inclusive QE electron-nucleus and CC neutrino-nucleus scattering processes. We restrict ourselves to the plane-wave Born approximation (PWBA) and assume the RIA. The analysis of scaling and superscaling with the general expressions implied is discussed in Sec. III. Here we also show the *experimental* scaling function together with a phenomenological fit and a comparison with the simple RFG result. In Sec. IV, we discuss the results starting with a global analysis of QE (e,e') reactions where off-shell effects in the differential cross sections are investigated at depth. We continue with the study of scaling properties, showing that our theoretical results do scale even when strong relativistic potentials are present. A separate analysis of the different channel contributions is also presented. Comparison with data shows that our model calculations do agree with experiment for specific descriptions of FSI. To conclude, we compare the scaling functions evaluated from (e,e') calculations with those obtained from (ν,μ) reactions [16]. Results show that they almost coincide, hence the model is consistent with the fulfillment of the universality property. Finally, in Sec. V we present our conclusions.

II. INCLUSIVE QUASIELASTIC LEPTON SCATTERING FORMALISM: THE RELATIVISTIC IMPULSE APPROXIMATION

This work deals with lepton induced reactions at energies of a few GeV and QE kinematics. In particular, we focus on inclusive electron scattering and CC neutrino (antineutrino) scattering on nuclei and assume the Born approximation (BA). The leptonic variables (in the laboratory system) involved in the processes are $K^\mu=(\varepsilon,\mathbf{k})$, the 4-momentum of the incident lepton (e or ν_μ) beam, and $K'^\mu=(\varepsilon',\mathbf{k}')$, the 4-momentum of the scattered lepton (e' or μ). The process is mediated by the exchange of a virtual photon (electron scattering) or a charged vector boson (CC neutrino scattering) with 4-momentum $Q^\mu=(K-K')^\mu=(\omega,\mathbf{q})$.

The general formalism for (e,e') and (ν,μ) reactions has been presented in previous works [4,8,13,15,21]. Here we simply summarize those basic aspects needed for later discussion. Assuming PWBA, i.e., one virtual particle exchanged and leptons described as free particles, the QE differential cross section can be expressed in terms of separate nuclear response functions. In the case of (e,e') reactions, we may write

$$\left[\frac{d\sigma}{d\varepsilon' d\Omega'}\right]_{(e,e')}=\sigma_M[v_L R^L(q,\omega)+v_T R^T(q,\omega)], \tag{1}$$

where Ω' is the scattered electron solid angle and the term σ_M represents the Mott cross section. Analogously, for CC neutrino scattering reactions the differential cross section can be written in the form [13,15]

$$\left[\frac{d\sigma}{d\varepsilon' d\Omega'}\right]_{\chi}=\sigma_0[\hat{v}_{CC}\hat{R}^{CC}+2\hat{v}_{CL}\hat{R}^{CL}+\hat{v}_{LL}\hat{R}^{LL}+\hat{v}_T\hat{R}^T+2\chi\hat{v}_{T'}\hat{R}^{T'}], \tag{2}$$

with (ε',Ω') the muon kinematic variables. The symbol χ specifies neutrino-induced reactions ($\chi=+$) or antineutrino-induced reactions ($\chi=-$), and the term σ_0 depends on the Fermi constant and the Cabibbo angle (see [13] for its explicit expression). The kinematic factors v_K and $\hat{v}_K$ come solely from the electromagnetic and weak leptonic tensors, respectively, and their explicit expressions can be found in [4,8,13].

The electromagnetic R^K and weak $\hat{R}^K$ response functions contain the whole dependence on the nuclear vertex coupling and are expressed by taking the appropriate components of the nuclear tensor [4,8,13]. This involves the matrix elements of the virtual photon or charged boson interaction with the nuclear electromagnetic or weak current. The inclusive hadronic electromagnetic tensor reads

$$W^{\mu\nu}(q,\omega)=\overline{\sum_i}\sum_f\delta(E_f-E_i-\omega)\langle f|\hat{J}^\mu_{\rm em}(Q)|i\rangle^*\times\langle f|\hat{J}^\nu_{\rm em}(Q)|i\rangle, \tag{3}$$

where $|i\rangle$ describes the initial target state and $|f\rangle$ represents a specific many-body final nuclear state. The term $\hat{J}^\mu_{\rm em}(Q)$ refers to the nuclear electromagnetic many-body current operator. A similar expression to (3) should be written for the weak tensor $\hat{W}^{\mu\nu}$ in terms of the nuclear weak many-body current operator $\hat{J}^\mu_w(Q)$. The electromagnetic tensor given in (3) is an exceedingly complicated object which includes all possible final states that can be connected with the initial ground state through the action of the many-body current operator.

In this paper, we restrict ourselves to the QE kinematic regime and we adopt the relativistic impulse approximation. Within the RIA, the many-body nuclear current operator is simply given as a sum of single-nucleon current operators that only couple the target ground state to scattering states lying in the one-body knockout space. The RIA approach has been extensively applied in investigations of exclusive electron scattering reactions [22–25]. Further details on the model for

neutrino-nucleus scattering reactions have been presented in [21,26–28]. Within the RIA framework, the main ingredient needed to evaluate the electromagnetic and weak tensor is the single-nucleon current matrix element,

$$\langle \hat{J}^\mu(Q)\rangle = \int d\mathbf{r} e^{i\mathbf{q}\cdot\mathbf{r}} \overline{\psi}_F(\mathbf{p}_F,\mathbf{r})\hat{\Gamma}^\mu \psi_B^{jm}(\mathbf{r}). \quad (4)$$

Here $\psi_B^{jm}(\mathbf{r})$ and $\psi_F(\mathbf{p}_F,\mathbf{r})$ are the wave functions for the initial (bound) nucleon and for the emitted nucleon, respectively, and $\hat{\Gamma}^\mu$ is the corresponding single-nucleon current operator for electron ($\hat{\Gamma}^\mu_{\rm em}$) or weak CC neutrino ($\hat{\Gamma}^\mu_w$) scattering.

We describe the bound nucleon states as self-consistent Dirac-Hartree solutions, derived within a relativistic mean field (RMF) approach using a Lagrangian containing σ, ω, and ρ mesons [29,30]. The outgoing nucleon state is described as a relativistic scattering wave function. Different options have been considered: first, the relativistic plane-wave impulse approximation (RPWIA), namely, the description of the knockout nucleons by means of plane-wave spinors; second, the effects due to FSI between the ejected nucleon and the residual nucleus. In our model, FSI effects are described by using Dirac equation solutions in the presence of relativistic potentials. This constitutes the relativistic distorted-wave impulse approximation (RDWIA) [22].

The use of energy-dependent complex relativistic optical potentials fitted to elastic proton scattering data has proven to be successful in describing *exclusive* $(e,e'p)$ scattering reactions under QE kinematics [22–25,31]. In this case of *exclusive* reactions, the optical potentials are built to reproduce the contribution from the elastic channel. For *inclusive* processes such as (e,e') and (ν,μ), the contribution from the inelastic channels should be retained. Ignoring them would lead to an underestimation of the inclusive cross section [27,32,33]. Multiple nucleon knockout effects have been treated in detail within the context of the Green function method [34–37]. A simple way of obtaining the inclusive strength within the RIA is to use purely real potentials. We consider two choices for the real part. The first uses the phenomenological relativistic optical potential from the energy-dependent, A-independent parametrizations (EDAIC, EDAIO, EDAICa) derived by Clark *et al.* [38], but with their imaginary parts set to zero. The second approach consists of describing the outgoing nucleon by means of distorted waves obtained with the same relativistic mean field used to describe the initial bound nucleon states. We refer to these two FSI descriptions as real relativistic optical potential (rROP) and RMF, respectively. Dispersion relation and Green function techniques [34–37] lead to results which are close to those obtained in the impulse approximation with either the rROP [36,37] or the mean field [34].

Concerning the current operator, we use the relativistic free nucleon expressions [13,39,40]. For electromagnetic (e,e') processes, the three usual options, denoted as CC1, CC2, and CC3, are considered:

$$\left[\hat{\Gamma}^\mu_{\rm CC1}\right]^{p(n)}_{\rm em} = \left(F_1^{p(n)} + F_2^{p(n)}\right)\gamma^\mu - \frac{F_2^{p(n)}}{2m_N}(\overline{P} + P_F)^\mu, \quad (5)$$

$$\left[\hat{\Gamma}^\mu_{\rm CC2}\right]^{p(n)}_{\rm em} = F_1^{p(n)}\gamma^\mu + \frac{iF_2^{p(n)}}{2m_N}\sigma^{\mu\nu}Q_\nu, \quad (6)$$

$$\left[\hat{\Gamma}^\mu_{\rm CC3}\right]^{p(n)}_{\rm em} = \frac{F_1^{p(n)}}{2m_N}\overline{P}^\mu + \frac{i\left(F_1^{p(n)} + F_2^{p(n)}\right)}{2m_N}\sigma^{\mu\nu}Q_\nu, \quad (7)$$

where $F_1^{p(n)}$ and $F_2^{p(n)}$ are the Pauli and Dirac proton (neutron) form factors, respectively, that depend only on Q^2, and the on-shell 4-momentum $\overline{P}^\mu = (\overline{E},\mathbf{p})$ with $\overline{E} = \sqrt{p^2 + m_N^2}$, and $\mathbf{p}$ the bound nucleon momentum has been introduced. Note that the three operators are equivalent for free on-shell nucleons (they are connected by the Gordon transformation). However, the RIA deals in general with off-shell bound and ejected nucleons. Hence the three operators lead to different results. Moreover, the current is not strictly conserved and uncertainties dealing with the election of gauge also occur [41–43].

The relativistic charged weak current of the nucleon is given as $\hat{\Gamma}^\mu_w = \hat{\Gamma}^\mu_V - \hat{\Gamma}^\mu_A$, where the vector and axial-vector current operators read

$$\hat{\Gamma}^\mu_V = F_1^V\gamma^\mu + i\frac{F_2^V}{2m_N}\sigma^{\mu\nu}Q_\nu, \quad (8)$$

$$\hat{\Gamma}^\mu_A = \left[G_A\gamma^\mu + \frac{G_P}{2m_N}Q^\mu\right]\gamma^5, \quad (9)$$

with $F_{1,2}^V$ the isovector nucleon form factors given in terms of the electromagnetic ones as $F_{1,2}^V = F_{1,2}^p - F_{1,2}^n$. The axial-vector and pseudoscalar form factors are parametrized as

$$G_A = \frac{g_A}{1 - Q^2/M_A^2}, \quad (10)$$

$$G_P = \frac{4m_N^2}{m_\pi^2 - Q^2}G_A, \quad (11)$$

with $g_A = 1.26$ and $M_A = 1032$ MeV (see [44,45]).

III. SCALING AND SUPERSCALING AT THE QUASIELASTIC PEAK

Detailed studies of scaling and superscaling for electron-nucleus cross sections have been presented in [3–5]. The analysis of the (e,e') world data has shown the quality of the scaling behavior: scaling of the first kind (no dependence on momentum transfer) is quite good at excitation energies below the QE peak, whereas scaling of the second kind (no dependence on nuclear species) works extremely well in the same region. In this paper, our aim is to investigate the QE scaling properties of electron-nucleus and CC neutrino-nucleus scattering within the context of the RIA. Assuming various RIA models, we prove that they do superscale, and we compare the associated scaling functions with the (e,e') phenomenological one.

In what follows, we present the basic expressions needed to get the scaling functions. Several choices have been proposed

in the literature for the appropriate scaling variable. Here, following the analysis of the RFG model, we adopt the dimensionless variable denoted as $\psi'(q,\omega)$,

$$\psi' \equiv \frac{1}{\sqrt{\xi_F}} \frac{\lambda' - \tau'}{\sqrt{(1+\lambda')\tau' + \kappa\sqrt{\tau'(1+\tau')}}}, \tag{12}$$

where $\lambda' \equiv (\omega - E_{\rm shift})/2m_N$, $\kappa \equiv q/2m_N$, $\tau' \equiv \kappa^2 - \lambda'^2$, and $\xi_F \equiv \sqrt{1+(k_F/m_N)^2} - 1$. The term k_F is the Fermi momentum, and the energy shift $E_{\rm shift}$, taken from [5], has been introduced to force the maximum of the cross section to occur for $\psi' = 0$. As usual, the notation ψ refers to the scaling variable when $E_{\rm shift} = 0$.

For inclusive QE electron scattering processes, the superscaling function is evaluated by dividing the differential cross section (1) by the appropriate single-nucleon eN elastic cross section weighted by the corresponding proton and neutron numbers [4,5,19] involved in the process. We may write

$$f(\psi', q) \equiv k_F \frac{\left[\dfrac{d\sigma}{d\varepsilon' d\Omega'}\right]_{(e,e')}}{\sigma_M \left[v_L G_L(q,\omega) + v_T G_T(q,\omega)\right]}. \tag{13}$$

The scaling behavior can also be analyzed by taking into account the separate electromagnetic longitudinal L and transverse T contributions. Thus the following scaling functions are introduced:

$$f_L(\psi', q) \equiv k_F \frac{R^L(q,\omega)}{G_L(q,\omega)}, \tag{14}$$

$$f_T(\psi', q) \equiv k_F \frac{R^T(q,\omega)}{G_T(q,\omega)}. \tag{15}$$

The single-nucleon functions G_L and G_T are given by

$$G_L = \frac{(\kappa^2/\tau)\left[\tilde{G}_E^2 + \tilde{W}_2\Delta\right]}{2\kappa\left[1 + \xi_F(1+\psi^2)/2\right]}, \tag{16}$$

$$G_T = \frac{2\tau\tilde{G}_M^2 + \tilde{W}_2\Delta}{2\kappa\left[1 + \xi_F(1+\psi^2)/2\right]}, \tag{17}$$

where the function Δ reads

$$\Delta = \xi_F(1-\psi^2)\left[\frac{\sqrt{\tau(1+\tau)}}{\kappa} + \frac{1}{3}\xi_F(1-\psi^2)\frac{\tau}{\kappa^2}\right]. \tag{18}$$

As usual, one has

$$\begin{aligned} &\tilde{G}_E^2 \equiv ZG_{Ep}^2 + NG_{En}^2, \quad \tilde{G}_M^2 \equiv ZG_{Mp}^2 + NG_{Mn}^2, \\ &\tilde{W}_2 = \frac{1}{1+\tau}\left[\tilde{G}_E^2 + \tau\tilde{G}_M^2\right], \end{aligned} \tag{19}$$

involving the proton and neutron form factors weighted by the proton and neutron numbers Z and N, respectively.

At sufficiently high energies, the function f depends only on the scaling variable ψ' but not on the transferred momentum q. Moreover, $f(\psi')$ becomes also independent of the momentum scale in the problem, that is, independent of k_F. The scaling behavior has been clearly demonstrated from the analysis of the QE (e, e') world data [3,4]. The investigation of the separate contribution of the longitudinal and transverse response functions has shown that scaling violations occur mainly in the T channel because of significant effects introduced by MEC, correlations, and inelastic scattering. From the global analysis presented in [3,4], a universal experimental superscaling function $f_{\rm exp}(\psi')$ has been defined. In Fig. 1, we present $f_{\rm exp}(\psi')$ averaged over the nuclei employed in the analysis, together with the corresponding fit. As noted, the experimental scaling function presents an asymmetric shape with a tail that extends toward positive values of the scaling variable ψ'. This is in contrast with the RFG superscaling function given by $f_{\rm RFG}(\psi') = (3/4)(1-\psi'^2)\theta(1-\psi'^2)$, that is symmetric, limited strictly to the region $|\psi'| \leqslant 1$, and with a maximum value of 3/4.

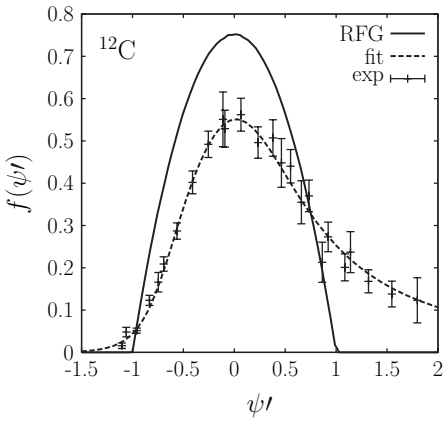

FIG. 1. RFG superscaling function compared to data and a parametrization of the results.

The general analysis of superscaling for CC neutrino-nucleus scattering has been presented in previous works [13,15,16]. Here, the superscaling function is obtained by dividing the differential cross section evaluated within the RIA (2) by the corresponding weak single-nucleon cross section as given explicitly in Eqs. (15), (45), (52), and (86)–(94) of [13]. Details and specific expressions are also given in Appendix C of [15]. This theoretical scaling function calculated from CC neutrino-nucleus cross sections can be compared directly with the one corresponding to (e, e') scattering calculations as well as with $f_{\rm exp}(\psi')$ shown above. This allows a check on the universality assumption of $f(\psi')$ and on the capabilities of different RIA models to yield the required properties of the experimental scaling function. By analogy to (e, e'), and in addition to the scaling function obtained from the CC neutrino-nucleus cross section, one may also construct the separate contributions given by the longitudinal L, transverse T, and axial-vector transverse T' responses, $f_{L,T,T'}(\psi')$. Here, the L weak response includes the contribution from the three terms in (2), namely, $\hat{v}_{CC}\hat{R}^{CC} + 2\hat{v}_{CL}\hat{R}^{CL} + \hat{v}_{LL}\hat{R}^{LL}$. In the next section, we present a detailed study of scaling and superscaling properties for (e, e') and (ν, μ) reactions within the RIA scheme.

IV. RESULTS

In this work, we consider the PWBA; i.e., Coulomb distortion of the leptons is neglected. Checks made for light-to-

medium nuclei within the *effective momentum approximation* [21,27] show that these effects are within a few percent for the high-energy lepton kinematics considered in this work. In this sense, our general conclusions about scaling are not modified by them. Obviously, the analysis of heavier nuclear systems requires a careful description of Coulomb distortion effects in the leptons (electrons and muons) involved in both processes (e, e') and (ν, μ).

A. Inclusive QE (e, e') reactions

1. Differential cross sections

In what follows, we present predictions for QE (e, e') reactions on ^{12}C within the framework of the RIA. Results correspond to fixed values of the incident electron beam energy $\varepsilon = 1$ GeV and scattering angle $\theta_e = 45^\circ$. The Lorentz gauge has been selected. In the next section, we present results for the scaling function concerning gauge effects. Figure 2 shows the differential cross section evaluated for the two current operators, CC1 and CC2, and FSI included through the rROP and RMF potentials. As observed, the CC1 choice leads to a significantly larger cross section, particularly within the RMF approach. Concerning FSI, the use of the RMF potential gives rise to a clear asymmetry in the cross section with a pronounced tail extending toward higher values of the transfer energy ω. For reference we also include in Fig. 2 the curve corresponding to RPWIA, i.e., no FSI. In such a case, the effects introduced by the current operator choice are minor. The difference observed between both FSI descriptions at high ω values is linked to the behavior of the two relativistic potentials: whereas the RMF contains strong energy-independent scalar and vector potentials, the energy dependence of the rROP makes its scalar and vector terms to be importantly reduced for high nucleon kinetic energies (high transfer energy). Hence, rROP results get close to the RPWIA ones for large ω values.

The asymmetry in the differential cross section is proved to be an effect entirely linked to the FSI description. Only in the presence of relativistic optical potentials with strong scalar and vector terms (RMF approach) is a significant shift

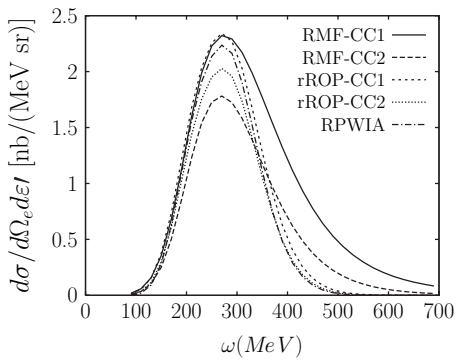

FIG. 2. Differential cross section for QE (e, e') on ^{12}C. FSI are described within the RMF and the rROP models. Results correspond to CC1 and CC2 current operators. For reference, the RPWIA result is presented. Incident electron energy $\varepsilon = 1$ GeV, scattering angle $\theta_e = 45^\circ$.

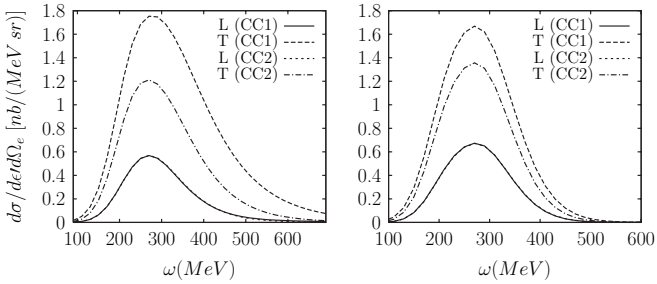

FIG. 3. Longitudinal L and transverse T contributions to the cross section. Left panel corresponds to RMF description of FSI; right panel to rROP. Results are presented for CC1 and CC2 prescriptions.

of strength to higher values of ω shown to occur. Details on the specific mechanism that produces the asymmetric tail in the cross section within the RMF-FSI approach are given in [46].

The importance of the current operator choice for the two FSI models is further investigated in Fig. 3, which presents a separate analysis of the longitudinal and transverse contributions to the cross section. As observed, the pure longitudinal response is almost identical with both current operators. In the case in which FSI are neglected, this result has been also found previously [41], and it was proven to be as due to the validity of the Gordon transformation for the longitudinal contributions. For the case of the transverse channel, the CC1 contribution is much larger than that of CC2 (likewise for CC3). Notice that the magnitude of this discrepancy depends on the specific FSI description, being larger for RMF, whereas in the plane-wave limit (RPWIA) both currents lead to very similar results. The ambiguity introduced by the current choice for inclusive (e, e') reactions has already been signaled in some previous works [47,48].

The large effects introduced by the current operator within the RMF (likewise for rROP) approach can also be analyzed by directly comparing theoretical and experimental cross sections. This may allow us to determine which particular choice is more appropriate. In Fig. 4, we compare data [49–54] with the results corresponding to the RIA-RMF approach with CC1 and CC2 at very different kinematics. As a general rule, we conclude that CC1 tends to overpredict data whereas the reverse applies to CC2. This outcome clearly favors the CC2 option in that the effects beyond the QE peak (Δ and MEC effects) may also play a significant role in the analysis of the data even at the maximum of the peak. However, data are not conclusive yet because the Δ and MEC contributions have not been evaluated.

2. Analysis of scaling behavior

The important effects already shown in the differential cross sections are also visible in the scaling function. In the following, we rely on the investigation of the superscaling properties and present results for the scaling function $f(\psi')$ (13), as well as the separate longitudinal and transverse contributions, i.e., $f_L(\psi')$ and $f_T(\psi')$. A comparison between the three scaling functions is presented in Fig. 5, where for simplicity only the RMF-FSI model has been considered.

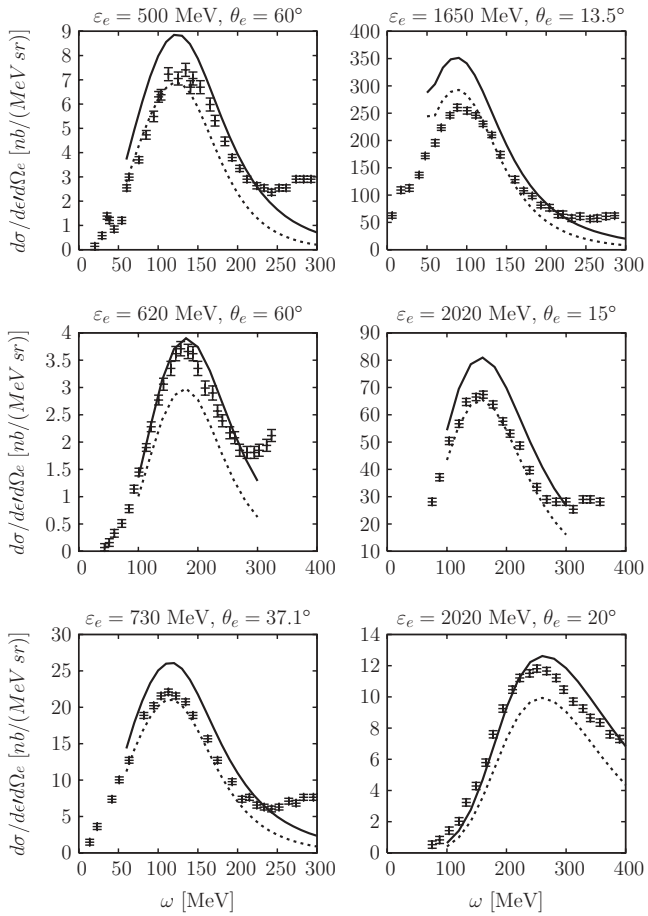

FIG. 4. Differential cross section for (e, e') reactions on ^{12}C. Theoretical predictions correspond to the RMF-FSI approach with CC1 (solid line) and CC2 (dashed line). Different kinematics (see labels) have been considered.

Similar conclusions are drawn for the rROP approach. In addition to the usual CC1 and CC2 prescriptions, we also include the results for the CC3 choice. As observed, the difference between $f(\psi')$ and the contributions $f_L(\psi')$ and $f_T(\psi')$ is very large for CC1, being much smaller for CC2 and almost negligible for CC3. This means that zero-kind scaling is fully broken for CC1 and RMF, whereas only a mild (negligible) violation is observed for CC2 (CC3). This behavior of the superscaling function is in accordance with the very diverse contributions given in the T channel by the different current operators. In particular, the CC1 current and RMF description of FSI lead to an important increase in the T channel strength compared with the single-nucleon contribution. On the contrary, the longitudinal function f_L is found to be basically the same for the three choices of the operator (likewise for rROP).

Scaling of the first kind is explored in Fig. 6, where we present $f(\psi')$ for three different values of the incident electron energy, $\varepsilon = 1, 1.5$, and 2 GeV. Results are shown for the two different descriptions of the FSI: RMF and rROP. In each case, we make predictions for the two usual current prescriptions, CC1 and CC2. As observed, the scaling function for the rROP model shows a very mild dependence on the

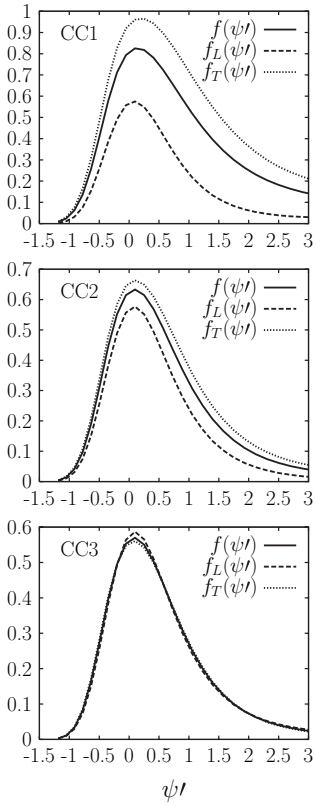

FIG. 5. Analysis of zero-kind scaling. Global scaling function $f(\psi')$ compared with separate L and T contributions. All results correspond to RMF description of FSI and current operators: CC1, CC2, and CC3.

transfer momentum in both positive and negative ψ' regions, i.e., first-kind scaling is well satisfied. In the case of the RMF model, a slight shift occurs in the "scaling region" $\psi' < 0$, whereas for ψ' positive, the model breaks scaling

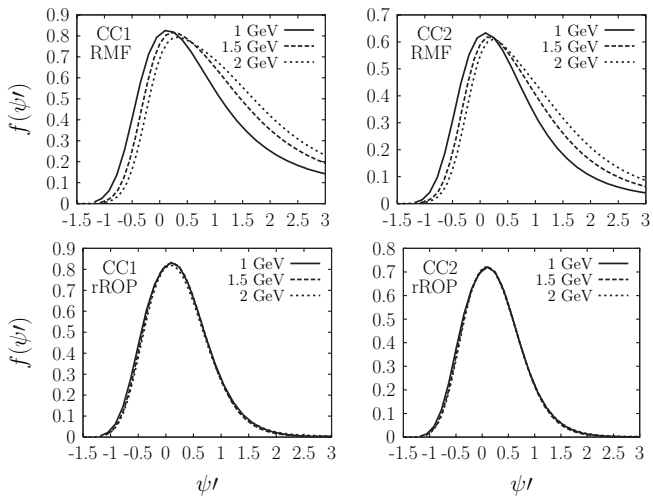

FIG. 6. Analysis of first-kind scaling. Scaling functions for three values of the incident electron energy. Kinematics and target as in previous figures. Results correspond to RMF and rROP models and the two choices of current operators: CC1 and CC2.

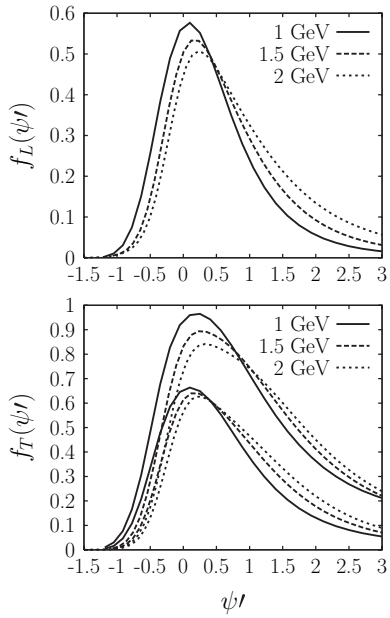

FIG. 7. Same as Fig. 6, but for the separate L and T contributions. Only the RMF approach is considered. In the case of the T response, the larger functions correspond to the CC1 operator and the smaller ones to CC2. In the L channel, almost no distinction is seen between the operators.

at roughly 30%. This violation is not in conflict with (e, e') data that indeed leave room for some violation of the first-kind scaling in this region, due partly to Δ production and partly to other contributions, such as MEC and correlations. A separate analysis of the L and T channels in the scaling function (see Fig. 7) shows that the breakdown of scaling within the RMF description of FSI is similar for both channels independently of which current choice is considered. In the case of rROP (and RPWIA) calculations, scaling of the first kind is excellent for all current operators and in both channels.

Scaling of the second-kind, i.e., independence of the specific nuclear system, is analyzed in Fig. 8. Here we present the results corresponding to CC1 and CC2 operators and the two descriptions of FSI: RMF and rROP. In each case, we compare the superscaling function evaluated for three different nuclei: ^{12}C, ^{16}O, and ^{40}Ca. The values of the Fermi momentum considered [5] correspond to $k_F = 216$ MeV/c (^{16}O), $k_F = 228$ MeV/c (^{12}C), and $k_F = 241$ MeV/c (^{40}Ca). As shown, the effects introduced by changing the nucleus are very small for the CC2 current choice and the two FSI descriptions. This is in complete accordance with data which show that second-kind scaling is excellent. On the contrary, the CC1 operator leads to a significant breakdown of scaling behavior which affects both FSI descriptions. This violation of the second-kind scaling comes totally from the transverse response. This is clearly illustrated in Fig. 9, where we present results for the separate functions $f_L(\psi')$ and $f_T(\psi')$ corresponding to the RMF model. Similar results are obtained for the rROP approach. From these theoretical results and the exhaustive analysis of the (e, e') world data, which proves the excellent quality of second-kind scaling behavior, one may question the validity of the CC1 operator used in describing QE (e, e') processes.

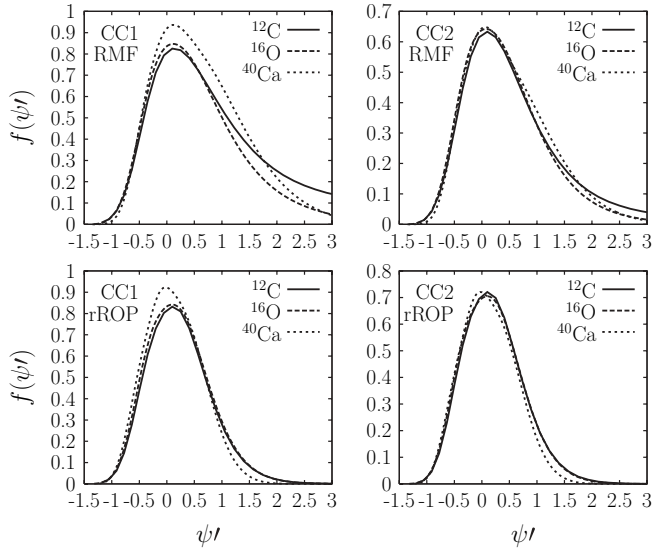

FIG. 8. Analysis of second-kind scaling. Scaling functions for ^{12}C, ^{16}O, and ^{40}Ca. Kinematics as in previous figures. Results for the RMF and rROP models are presented for CC1 and CC2 prescriptions.

3. Comparison with experiment

A comparison between the theoretical superscaling functions and the averaged QE phenomenological function obtained from the analysis of (e, e') data is presented in Fig. 10. We have selected the CC2 operator and show results for the three different descriptions of the continuum final state, namely, the RPWIA, rROP, and RMF. Lorentz gauge has been assumed. The symmetric character of the RPWIA and rROP curves differs clearly from the experimental analysis. On the contrary, the RMF approach displays an asymmetric shape with a long tail extended to positive values of the

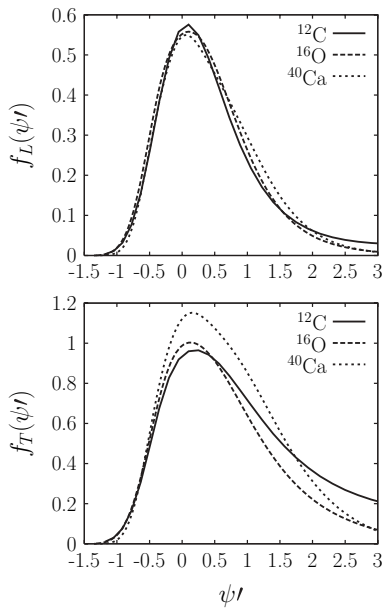

FIG. 9. Separate L and T contributions to second-kind scaling analysis. Results correspond only to the RMF model.

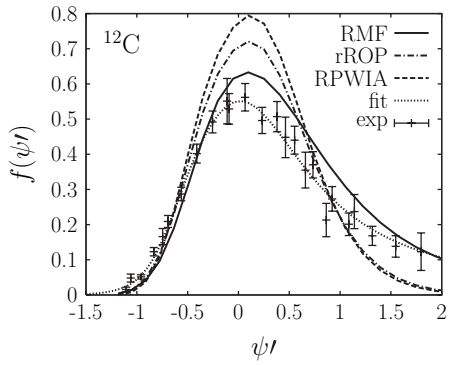

FIG. 10. Scaling function for ^{12}C(e, e') evaluated with the RPWIA, rROP, and RMF approaches compared to experimental function together with a phenomenological parametrization.

scaling variable ψ' which follows closely the behavior of the phenomenological function. As already mentioned in previous work [16], this asymmetry of the RMF description constitutes a basic difference from other models presented in the literature [55–57] where the long tail in $f(\psi')$ is largely absent.

The asymmetry in data has usually been ascribed to ingredients beyond the mean field, such as short-range correlations, induced nonlocalities, and two-body currents. Within a nonrelativistic aproach, such ingredients are needed in order to get the asymmetry [17,18,58]. However, here we show that a large amount of the asymmetry is indeed obtained within the framework of the RIA and a RMF description of the final continuum nucleon states. This is in accordance with some previous works [59–62] where a comparison between Dirac-Brueckner-Hartree-Fock (DBHF) and Dirac-Hartree calculations indicates that effects from correlations and Fock terms in the DBHF calculation can be accounted for by the simple Dirac-Hartree approach fitted to saturation properties of nuclear matter. This is at variance with the nonrelativistic mean field case. In this respect, note that the Dirac equation in the presence of scalar and vector local potentials can be reduced to a nonrelativistic Schrödinger-like equation with energy-dependent and nonlocal terms [23]. Results in Fig. 10 show that the asymmetry in the scaling function can be produced via local, energy-independent relativistic potentials within the impulse approximation, and moreover, such asymmetry is very close to the experiment. This outcome does not contradict the additional role that may be played by correlations and exchange currents not accounted for within the relativistic mean field calculation. However, the small magnitude of the local central and spin-orbit potentials involved in the nonrelativistic approach cannot yield a significant asymmetry. Only a strong nonlocality of the potentials (effective values of the mass and energy) may give rise to an *asymmetric* differential cross section [46].

To complete the analysis, in Fig. 11 (left panels) we select the RMF description of FSI and compare data and the fit curve with the theoretical results for the three choices of the current operator: CC1, CC2, and CC3. In each case, we also present a separate analysis of the L and T channels involved in the process. As already shown in previous results, the longitudinal contribution $f_L(\psi')$ does not depend on the

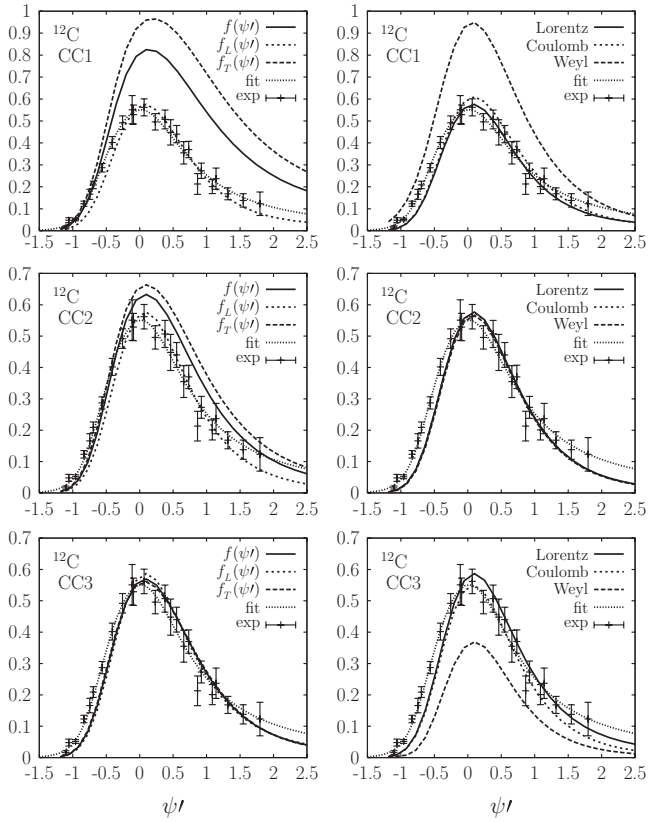

FIG. 11. Scaling functions evaluated for different currents and gauges compared to experiment. Left panels show $f(\psi')$ as well as the contributions $f_L(\psi')$ and $f_T(\psi')$ for the three current choices and the gauge fixed to Lorentz. Right panels show the results for the longitudinal scaling function $f_L(\psi')$ for the three currents and the three gauges: Lorentz, Coulomb, and Weyl.

current operator choice and agrees nicely with experiment. On the contrary, the strength of the transverse response with the CC1 current leads to a function $f_T(\psi')$ that is roughly twice the data. Discrepancies between $f_L(\psi')$ and $f_T(\psi')$ are mild (negligible) for CC2 (CC3) leading to a global scaling function $f(\psi')$ which is in accord in both cases with the experiment. All the curves presented for the longitudinal contribution $f_L(\psi')$ satisfy the Coulomb sum rule, i.e., they integrate to unity.

Up to now we have only discussed calculations corresponding to the Lorentz gauge. Results for the Coulomb gauge are similar for all FSI descriptions, whereas the Weyl gauge leads in most of the cases to very important discrepancies. This is clearly illustrated in the right panels of Fig. 11 where we show the longitudinal scaling function $f_L(\psi')$ evaluated for the three gauges and the three current operator choices. The RMF approach for the final state has been assumed. The discussion of results follows in general similar trends for the rROP model. Note that the gauge only affects the longitudinal response. As observed in Fig. 11, Lorentz and Coulomb gauges lead to very close results for all currents, particularly for CC2, where there is no distinction between the two curves. In the case of the Weyl gauge, an important difference emerges between the CC2 operator and the other two, CC1 and CC3. In the former, the scaling function $f_L(\psi')$ is almost the same for

the three gauges. This is in accordance with the fact that the continuity equation is highly fulfilled within the RMF model and the CC2 current operator. By contrast, the CC1 and CC3 operators within the Weyl gauge give rise to longitudinal scaling functions which depart significantly from data being much larger (smaller) for CC1 (CC3). In both cases the Coulomb sum rule is clearly violated. These results reinforce our confidence in the adequacy of descriptions of inclusive (e, e') reactions when based on the RMF-FSI approach and the CC2 current operator. Only in this case, the results do not depend on the specific gauge selected;[1] moreover, they are also shown not to be modified by the dynamic enhancement of the lower components [46].

B. Inclusive QE charged-current (ν, μ) reactions

The analysis of scaling and superscaling for CC neutrino-nucleus reactions has been presented in [13,16]. It is important to point out that any reliable calculation of neutrino-nucleus cross sections must first be tested against electron scattering data. Hence, two different approaches can be pursued. First, using the scaling behavior of (e, e') cross sections and the universality property of the superscaling function, we can make predictions for inclusive (ν, μ) reactions by taking the empirical electron scattering scaling function $f_{\rm exp}(\psi')$. This strategy, applied not only to the QE regime but also to the Δ kinematic region, was analyzed at depth in [13]. The second approach, considered in [16], consists of evaluating explicitly $f(\psi')$ for (ν, μ) reactions within a specific model, namely, RDWIA. The scaling function obtained in this way can be compared directly with the model predictions given for (e, e') processes. This allows us to check not only the scaling behavior of the calculations, but also the consistency of the universality assumption of $f(\psi')$ and the capability of the model to reproduce the experimental data.

In [16], we presented a detailed investigation of CC neutrino-nucleus scattering reactions within the RIA framework. We proved that superscaling is verified to high accuracy by the model calculations even in the presence of strong relativistic potentials. Importantly, the results obtained when FSI were described by means of the RMF potential presented the right asymmetry compared with data. This is fully consistent with the discussion outlined in the previous section concerning the study of inclusive (e, e') reactions. This consistency is clearly illustrated in Fig. 12, which compares the scaling functions evaluated from (e, e') and (ν, μ) reactions. We only consider the RMF-FSI case as this is the only model which is in accordance with data. However, the consistency between electron and neutrino scattering calculations applies also to rROP and RPWIA approaches. In the left panel of Fig. 12, the CC2 prescription has been assumed for (e, e') and the separate contributions of both channels, L and T, are also shown. For completeness, the case of the CC3 operator is

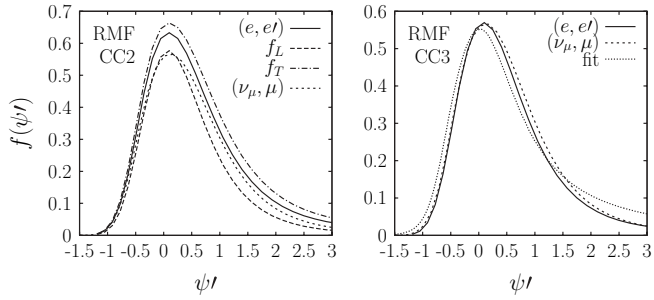

FIG. 12. Consistency of scaling functions evaluated for (e, e') and (ν, μ) reactions for CC2 and CC3 current choices. Incident electron (neutrino) energy is fixed to 1 GeV and the scattering angle to 45°. Separate L and T contributions are also presented.

considered in the right panel, and the fit curve to experiment is also drawn for reference. From these results, it is clear that the universality assumption of the scaling function is highly fulfilled within the present RIA model. This supports the use of the experimental (e, e') scaling function in order to predict reliable neutrino-nucleus scattering cross sections [13].

Although not presented for simplicity, a separate analysis of the various channels, L, T, and T', contributing to (ν, μ) reactions shows that $f_T(\psi') = f_{T'}(\psi') = f(\psi')$, i.e., scaling of zero kind is verified. The longitudinal contribution leads to a scaling function $f_L(\psi')$ which departs significantly from $f(\psi')$. However, one should be cautious because the L contribution to inclusive (ν, μ) cross sections is almost negligible compared with the transverse, T, T', ones.

To conclude with the analysis of results, we present again in Fig. 13 the scaling function predictions for both (e, e') and (ν, μ) reactions with the RMF description in the final state, and compare them with data and the fit curve. Here we use a logarithmic scale in $f(\psi')$ in order to enlarge the discrepancies between theory and experiment in the scaling region, i.e., negative ψ' values. In this region, our model predictions for electron and neutrino processes are in full agreement and tend to underpredict the data. This is not unexpected because the model is entirely based on one-body phase space. Ingredients beyond the impulse approximation, i.e., multinucleon knockout, either induced by exchange currents, correlations, or rescattering effects, are surely needed to get more strength in the scaling function which will be then closer to the experiment. This is in fact the case of the coherent density fluctuation model (CDFM) for correlations presented in [55–57]. This model is an extension of the RFG applied to finite nuclei, and its prediction is also shown for comparison in Fig. 13. The CDFM result, compared with the RMF calculations, presents more strength in the negative ψ' region, being closer to data. However, CDFM is manifestly symmetrical around the QE peak.[2] As discussed in previous sections, the asymmetry of the scaling function comes mainly from the inclusion of FSI in the reaction mechanism. This

[1] Although not shown, the Weyl gauge leads to different results when the rROP model is assumed independently of the current operator selected.

[2] The author is aware of a new development of the CDFM model in which asymmetry is incorporated in an effective way [63].

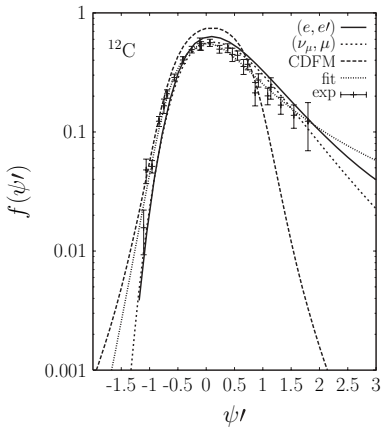

FIG. 13. Same as Fig. 12, but in logarithmic scale. We also include data and compare with the predictions given by the CDFM model.

ingredient, when based on the RMF description, gives rise to the right asymmetry shown by the experiment.

A detailed analysis of scaling and cross sections within a nonrelativistic mean field approach has been presented in [15]. In Fig. 14, we compare CC neutrino-nucleus cross sections obtained with the RIA model and the semirelativistic (SR) one developed in [15]. The SR approach includes important relativistic ingredients in the current operator. This has been already illustrated in previous works [9,15,64,65], and it is also clearly shown by results in Fig. 14 corresponding to the plane-wave limit; the fully relativistic and the SR calculations lead to very similar curves in spite of using different descriptions of the initial bound nucleon wave functions: solutions of the Dirac-Hartree model and the Schrödinger equation with a Woods-Saxon potential, respectively. On the contrary, relativistic and SR results are very different when FSI are included by using potentials (RMF and Woods-Saxon) in the final state. Whereas the RMF shows a significant asymmetry, the SR-FSI approach shifts the SR-PWIA result to higher muon energies, but maintains the global symmetry of the cross section [8,15]. Asymmetry within the nonrelativistic

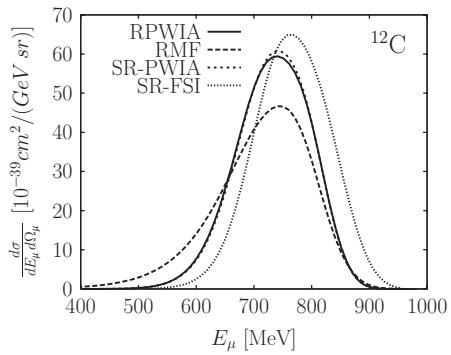

FIG. 14. Predictions for ^{12}C(ν,μ) differential cross sections. The RIA model is compared with the SR approach. Two different descriptions of FSI have been considered. First the plane-wave limit, which leads to very similar results. Second FSI described by means of the RMF model (dashed) and making use of a Woods-Saxon potential in the SR framework (dotted).

framework requires ingredients in the final state beyond the impulse approximation and mean field picture: correlations, nonlocalities, exchange terms, and multinucleon emission. By contrast, most of the asymmetry involved in the experiment is already obtained within a simple, fully relativistic mean field model based on the impulse approximation and describing FSI by means of strong local scalar and vector potentials. This makes a crucial difference between both relativistic and nonrelativistic descriptions.

V. CONCLUSIONS

In this paper, we have presented a global study of scaling and superscaling properties concerning inclusive QE electron and CC neutrino-nucleus scattering reactions. The general framework in which the calculations have been performed is the RIA. This is a simplified description of the reaction mechanisms because it presupposes that the processes to be calculated depend entirely on one-body phase space. However, in spite of its simplicity, the RIA has been used to describe successfully QE $(e,e'N)$ reactions. For the inclusive (e,e') and (ν,μ) processes we are interested in, a crucial ingredient is the description of FSI. We have considered different options consistent with retaining in the calculations the contribution from the inelastic channels. This is provided in our model by using purely real potentials. Three different cases have been explored: (i) the plane-wave limit, (ii) using the real part of the energy-dependent relativistic optical potentials parametrized by Clark *et al.* [38], and (iii) employing the same relativistic mean field potential considered in the description of the initial bound nucleon states.

The differential (e,e') cross sections are shown to be very sensitive to some ingredients of the model, particularly, the specific current operator selected (CC1 vs CC2) and the relativistic FSI description. The former, off-shell effects, enter essentially into the transverse channel, whereas the longitudinal one shows a very mild dependence on the current operator choice. Concerning FSI, a basic difference emerges when comparing the rROP and RMF approaches to the cross section. The latter presents a significant asymmetry extended to higher values of the transfer energy. The origin of this effect is directly linked to the use of very strong relativistic optical potentials [46].

The main goal of this paper is centered on the analysis of the scaling behavior of the cross sections and separate responses. Our results show that scaling of zero order is verified for the CC2 and CC3 current operators; however, the CC1 leads to an important breakdown of scaling because of the extremely large contribution given by the transverse response. This outcome is strictly true when FSI effects are taken into account. In the plane-wave limit (RPWIA), results present a mild dependence on the current operator. Concerning first-kind scaling, i.e., independence of the transfer momentum, all our results satisfy this property, which is in accord with the general behavior of data. Being more precise, only in the case of FSI described with the RMF potential does the superscaling function show some dependence on the transfer momentum. However, this scaling breakdown is compatible with (e,e')

data. A separate analysis of the two channels involved in the calculations leads to similar conclusions.

A special comment should be made concerning second-kind scaling, i.e., independence of the nuclear species. Recent analyses of (e, e') data conclude that this property is excellent, showing only a small scaling violation in the region above the QE peak (positive ψ' values). This means that any theoretical model that does not satisfy this behavior should be dismissed, or at least, clearly disfavored. In our model, the analysis performed shows that the use of the CC1 operator leads to a visible breakdown of second-kind scaling. This applies to both FSI descriptions, rROP and RMF, and it comes totally from the transverse response. These results strongly favor the use of the CC2 (likewise CC3) operator, which agrees with some general comments made in the past concerning the analysis of *exclusive* QE $(e, e'p)$ data at high missing momentum values [24]. Note that second-kind scaling is highly fulfilled for the longitudinal contribution $f_L(\psi')$.

A comparison with the *phenomenological* scaling function extracted from (e, e') data shows that only the FSI description based on the RMF approach leads to the right amount of asymmetry. Within the one-body context, this significant shift of strength to positive ψ' values only occurs in the presence of strong scalar and vector relativistic optical potentials. This is the case of the energy-independent RMF approach. On the contrary, the energy-dependent scalar and vector terms in the rROP are importantly reduced for increasing outgoing nucleon energies (positive ψ' region). Comparison with data indicates that the RMF-FSI model incorporates important dynamic effects missed by other models. In a nonrelativistic approach, the asymmetry can be only generated by including ingredients beyond the impulse approximation. Here we show that a simple local, energy-independent relativistic mean field potential takes care of the basic behavior presented by (e, e') data.

The gauge analysis performed in this work leads to an important conclusion concerning the RMF-FSI approach. Notice that gauge ambiguity only affects the longitudinal contribution $f_L(\psi')$. Our study shows that Coulomb and Lorentz gauges give rise to very similar results, being in general significantly different from the Weyl ones. However, in the particular case of FSI described with the RMF potential and the CC2 current operator selected, the longitudinal scaling function does not show sensitivity to the gauge election. Only in this situation, the results of f_L are very similar for the three gauges and, more importantly, all of them essentially satisfy the Coulomb sum rule, i.e., they integrate to unity. By contrast, for CC1 and CC3 prescriptions, the Weyl f_L results deviate significantly from the other gauges, breaking also the Coulomb sum rule. This general result gives us confidence in the adequacy of descriptions of QE (e, e') reactions when based on the RMF-FSI approach and the CC2 current operator. This choice, in addition to be mostly insensitive to gauge ambiguities and dynamic relativistic effects, leads to the *correct* asymmetry shown by data.

To conclude, we have compared the scaling function evaluated from (e, e') calculations with that obtained from (ν, μ) reactions. The results for both processes are very close, and this is fully consistent with the general statement on the universality property of the scaling function. Within the RIA framework, the superscaling function is basically the same for the two t-channel processes considered. This supports the general approach considered in [13], i.e., the use of the scaling function extracted from (e, e') data to predict neutrino-nucleus cross sections. It will be very interesting in the future to determine if the universality property emerges also from RIA calculations applied to NC neutrino-nucleus scattering reactions [20].

ACKNOWLEDGMENTS

This work has benefited from very fruitful discussions with J. E. Amaro, M. B. Barbaro, T. W. Donnelly, E. Moya de Guerra, and J. M. Udías. I warmly thank all of them. I also acknowledge A. N. Antonov for providing the CDFM scaling function. This work was partially supported by funds provided by Ministerio de Educación y Ciencia (Spain) and FEDER funds, under Contracts Nos. FPA2005-04460 and FIS2005-01105, by the Junta de Andalucía, and by the INFN-CICYT collaboration agreements no. 05-22.

[1] G. B. West, Phys. Rep. **18**, 263 (1975).
[2] D. B. Day, J. S. McCarthy, T. W. Donnelly, and I. Sick, Annu. Rev. Nucl. Part. Sci. **40**, 357 (1990).
[3] T. W. Donnelly and I. Sick, Phys. Rev. Lett. **82**, 3212 (1999).
[4] T. W. Donnelly and I. Sick, Phys. Rev. C **60**, 065502 (1999).
[5] C. Maieron, T. W. Donnelly, and I. Sick, Phys. Rev. C **65**, 025502 (2002).
[6] L. Alvarez-Ruso, M. B. Barbaro, T. W. Donnelly, and A. Molinari, Nucl. Phys. **A724**, 157 (2003).
[7] M. B. Barbaro, J. A. Caballero, T. W. Donnelly, and C. Maieron, Phys. Rev. C **69**, 035502 (2004).
[8] J. E. Amaro, M. B. Barbaro, J. A. Caballero, T. W. Donnelly, and A. Molinari, Nucl. Phys. **A697**, 388 (2002).
[9] J. E. Amaro, M. B. Barbaro, J. A. Caballero, T. W. Donnelly, and A. Molinari, Phys. Rep. **368**, 317 (2002).
[10] J. E. Amaro, M. B. Barbaro, J. A. Caballero, T. W. Donnelly, and A. Molinari, Nucl. Phys. **A723**, 181 (2003).
[11] A. De Pace, M. Nardi, W. M. Alberico, T. W. Donnelly, and A. Molinari, Nucl. Phys. **A726**, 303 (2003).
[12] A. De Pace, M. Nardi, W. M. Alberico, T. W. Donnelly, and A. Molinari, Nucl. Phys. **A741**, 249 (2004).
[13] J. E. Amaro, M. B. Barbaro, J. A. Caballero, T. W. Donnelly, A. Molinari, and I. Sick, Phys. Rev. C **71**, 015501 (2005).
[14] W. M. Alberico, A. Molinari, T. W. Donnelly, E. L. Kronenberg, and J. W. Van Orden, Phys. Rev. C **38**, 1801 (1988).
[15] J. E. Amaro, M. B. Barbaro, J. A. Caballero, T. W. Donnelly, and C. Maieron, Phys. Rev. C **71**, 065501 (2005).
[16] J. A. Caballero, J. E. Amaro, M. B. Barbaro, T. W. Donnelly, C. Maieron, and J. M. Udías, Phys. Rev. Lett. **95**, 252502 (2005).

[17] G. Co', C. Bleve, I. De Mitri, and D. Martello, Nucl. Phys. Proc. Suppl. **112**, 210 (2002).
[18] C. Bleve *et al*., Astropart. Phys. **16**, 145 (2001).
[19] M. B. Barbaro, R. Cenni, A. De Pace, T. W. Donnelly, and A. Molinari, Nucl. Phys. **A643**, 137 (1998).
[20] J. E. Amaro, M. B. Barbaro, J. A. Caballero, and T. W. Donnelly, Phys. Rev. C **73**, 035503 (2006).
[21] W. M. Alberico *et al*., Nucl. Phys. **A623**, 471 (1997).
[22] J. M. Udías, P. Sarriguren, E. Moya de Guerra, E. Garrido, and J. A. Caballero, Phys. Rev. C **48**, 2731 (1993); J. M. Udías, Ph.D. thesis, Univ. Autónoma Madrid, 1993.
[23] J. M. Udías, P. Sarriguren, E. Moya de Guerra, E. Garrido, and J. A. Caballero, Phys. Rev. C **51**, 3246 (1995).
[24] J. M. Udías, P. Sarriguren, E. Moya de Guerra, and J. A. Caballero, Phys. Rev. C **53**, R1488 (1996).
[25] J. M. Udías, J. A. Caballero, E. Moya de Guerra, J. R. Vignote, and A. Escuderos, Phys. Rev. C **64**, 024614 (2001).
[26] W. M. Alberico *et al*., Phys. Lett. **B438**, 9 (1998); Nucl. Phys. **A651**, 277 (1999).
[27] C. Maieron, M. C. Martínez, J. A. Caballero, and J. M. Udías, Phys. Rev. C **68**, 048501 (2003).
[28] M. C. Martínez, P. Lava, N. Jachowicz, J. Ryckebusch, K. Vantournhout, and J. M. Udías, Phys. Rev. C **73**, 024607 (2006).
[29] C. J. Horowitz and B. D. Serot, Nucl. Phys. **A368**, 503 (1981); Phys. Lett. **B86**, 146 (1979).
[30] B. D. Serot and J. D. Walecka, Adv. Nucl. Phys. **16**, 1, edited by J. W. Negele and E. W. Vogt (Plenum Press, New York, 1986).
[31] J. J. Kelly, *Advances in Nuclear Physics*, edited by J. W. Negele and E. W. Vogt (Plenum Press, New York, 1996), Vol. 23, p. 75 and references therein; J. D. Walecka, *Electron Scattering for Nuclear and Nucleon Structure* (Cambridge University Press, Cambridge, 2001).
[32] Y. Jin, D. S. Onley, and L. E. Wright, Phys. Rev. C **45**, 1333 (1992).
[33] K. S. Kim and L. E. Wright, Phys. Rev. C **68**, 027601 (2003); **72**, 064607 (2005).
[34] Y. Horikawa, F. Lenz, and N. C. Mukhopadhyay, Phys. Rev. C **22**, 1680 (1980).
[35] C. R. Chinn, A. Picklesimer, and J. W. Van Orden, Phys. Rev. C **40**, 790 (1989).
[36] A. Meucci, F. Capuzzi, C. Giusti, and F. D. Pacati, Phys. Rev. C **67**, 054601 (2003).
[37] A. Meucci, C. Giusti, and F. D. Pacati, Nucl. Phys. **A739**, 277 (2004).
[38] E. D. Cooper, S. Hama, B. C. Clark, and R. L. Mercer, Phys. Rev. C **47**, 297 (1993).
[39] M. C. Martínez, J. A. Caballero, T. W. Donnelly, Nucl. Phys. **A707**, 83 (2002) and refs. therein.
[40] T. de Forest, Nucl. Phys. **A392**, 232 (1983).
[41] J. A. Caballero, T. W. Donnelly, E. Moya de Guerra, and J. M. Udías, Nucl. Phys. **A643**, 189 (1998); **A632**, 323 (1998).
[42] J. M. Udías, J. A. Caballero, E. Moya de Guerra, J. E. Amaro, and T. W. Donnelly, Phys. Rev. Lett. **83**, 5451 (1999).
[43] M. C. Martínez, J. R. Vignote, J. A. Caballero, T. W. Donnelly, E. Moya de Guerra, and J. M. Udías, Phys. Rev. C **69**, 034604 (2004).
[44] W. M. Alberico, S. M. Bilenky, and C. Maieron, Phys. Rep. **358**, 227 (2002).
[45] V. Bernard, L. Elouadrhiri, and U. G. Meissner, J. Phys. G **28**, R1 (2002).
[46] J. M. Udías (private communication).
[47] H. Kim, C. J. Horowitz, and M. R. Frank, Phys. Rev. C **51**, 792 (1995).
[48] C. R. Chinn, Phys. Rev. C **50**, 1509 (1994).
[49] A. V. Butkevich and S. P. Mikheyev, Phys. Rev. C **72**, 025501 (2005).
[50] R. Whitney *et al*., Phys. Rev. C **9**, 2230 (1974).
[51] J. S. O'Connell *et al*., Phys. Rev. C **35**, 1063 (1987).
[52] P. Barreau *et al*., Nucl. Phys. **A402**, 515 (1983).
[53] D. Baran *et al*., Phys. Rev. Lett. **61**, 400 (1988).
[54] D. B. Day *et al*., Phys. Rev. C **48**, 1849 (1993).
[55] A. N. Antonov, M. K. Gaidarov, D. N. Kadrev, M. V. Ivanov, E. M. de Guerra, and J. M. Udías, Phys. Rev. C **69**, 044321 (2004).
[56] A. N. Antonov, M. K. Gaidarov, M. V. Ivanov, D. N. Kadrev, E. Moya de Guerra, P. Sarriguren, and J. M. Udías, Phys. Rev. C **71**, 014317 (2005).
[57] A. N. Antonov, M. V. Ivanov, M. K. Gaidarov, E. Moya de Guerra, P. Sarriguren, and J. M. Udías, Phys. Rev. C **73**, 047302 (2006); **73**, 059901(E) (2006).
[58] J. Nieves, J. E. Amaro, and M. Valverde, Phys. Rev. C **70**, 055503 (2004).
[59] A. Trasobares, A. Polls, A. Ramos, and H. Müther, Nucl. Phys. **A640**, 471 (1998).
[60] M. Kleinmann, R. Fritz, H. Müther, and A. Ramos, Nucl. Phys. **A579**, 85 (1994).
[61] E. Schiller and H. Müther, Eur. Phys. J. A **11**, 15 (2000) and refs. therein.
[62] M. M. Sharma, M. A. Nagarajan, and P. Ring, Phys. Lett. **B312**, 377 (1993).
[63] A. N. Antonov *et al*., submitted to Phys. Rev. C. (July 2006).
[64] J. E. Amaro, J. A. Caballero, T. W. Donnelly, A. M. Lallena, E. Moya de Guerra, and J. M. Udías, Nucl. Phys. **A602**, 263 (1996).
[65] J. E. Amaro, J. A. Caballero, T. W. Donnelly, and E. Moya de Guerra, Nucl. Phys. **A611**, 163 (1996).